

Patterned Optoelectronic Tweezers: A New Scheme for Selecting, Moving, and Storing Dielectric Particles and Cells

Shuailong Zhang, Nika Shakiba, Yujie Chen, Yanfeng Zhang, Pengfei Tian, Jastaranpreet Singh, M. Dean Chamberlain, Monika Satkauskas, Andrew G. Flood, Nazir P. Kherani, Siyuan Yu, Peter W. Zandstra, and Aaron R. Wheeler*

Optical micromanipulation has become popular for a wide range of applications. In this work, a new type of optical micromanipulation platform, patterned optoelectronic tweezers (p-OET), is introduced. In p-OET devices, the photoconductive layer (that is continuous in a conventional OET device) is patterned, forming regions in which the electrode layer is locally exposed. It is demonstrated that micropatterns in the photoconductive layer are useful for repelling unwanted particles/cells, and also for keeping selected particles/cells in place after turning off the light source, minimizing light-induced heating. To clarify the physical mechanism behind these effects, systematic simulations are carried out, which indicate the existence of strong nonuniform electric fields at the boundary of micropatterns. The simulations are consistent with experimental observations, which are explored for a wide variety of geometries and conditions. It is proposed that the new technique may be useful for myriad applications in the rapidly growing area of optical micromanipulation.

1. Introduction

Optical micromanipulation technologies such as optical tweezers and optoelectronic tweezers have become popular for a variety of applications.^[1–5] For example, optical micromanipulation technologies are useful for studying the behavior of microorganisms such as bacteria and *Caenorhabditis elegans*,^[6–10] the evaluation of molecular dynamics and mechanics,^[11–14] and the positioning and sorting of mammalian cells.^[15–21] The first optical micromanipulation technology was demonstrated by Arthur Ashkin et al. in 1986,^[22] a method commonly known as optical tweezers (OT). In this technique, a high numerical aperture lens is used to apply an optical gradient force


Dr. S. Zhang, Dr. N. Shakiba, Dr. M. D. Chamberlain, M. Satkauskas, Prof. P. W. Zandstra, Prof. A. R. Wheeler
Donnelly Centre for Cellular and Biomolecular Research
University of Toronto
Toronto, ON M5S 3E1, Canada
E-mail: aaron.wheeler@utoronto.ca

Dr. S. Zhang, Dr. M. D. Chamberlain, M. Satkauskas, Prof. A. R. Wheeler
Department of Chemistry
University of Toronto
Toronto, ON M5S 3H6, Canada

Dr. S. Zhang, Dr. N. Shakiba, Dr. J. Singh, Dr. M. D. Chamberlain, Prof. P. W. Zandstra, Prof. A. R. Wheeler
Institute for Biomaterials and Biomedical Engineering
University of Toronto
Toronto, ON M5S 3G9, Canada

Dr. Y. Chen, Dr. Y. Zhang, Prof. S. Yu
State Key Laboratory of Optoelectronic Materials and Technologies
School of Electronics and Information Technology
Sun Yat-sen University
Guangzhou 510275, China

Dr. P. Tian
Institute for Electric Light Sources
Fudan University
Shanghai 200433, China

 The ORCID identification number(s) for the author(s) of this article can be found under <https://doi.org/10.1002/sml.201803342>.

A. G. Flood, Prof. N. P. Kherani
Department of Electrical and Computer Engineering
University of Toronto
Toronto, ON M5S 3G4, Canada

Prof. N. P. Kherani
Department of Materials Science and Engineering
University of Toronto
Toronto, ON M5S 3E4, Canada

Prof. S. Yu
Photonics Group
Merchant Venturers School of Engineering
University of Bristol
Bristol BS81UB, UK

Prof. P. W. Zandstra
Medicine by Design
University of Toronto
Toronto, ON M5S 3G9, Canada

Prof. P. W. Zandstra
School of Biomedical Engineering
University of British Columbia
Vancouver, BC V6T 1Z3, Canada

Prof. P. W. Zandstra
Michael Smith Laboratories
University of British Columbia
Vancouver, BC V6T 1Z3, Canada

DOI: 10.1002/sml.201803342

to an object, allowing for the transfer of optical momentum to control its position.^[23–25] Optoelectronic tweezers (OET) is a related but distinct technique that was first demonstrated by Ming Wu and co-workers in 2005,^[4] relying on photoconductor-coated substrates that are typically insulating, but can be made to be conductive upon illuminating with light. OET has been applied to manipulating nanowires, nanotubes, nanoparticles, dielectric beads, and living cells.^[26–35] Because OET relies on light to control the application of dielectrophoresis (DEP) forces rather than relying on the photons themselves to generate force, OET systems typically exert a much stronger manipulation force for a given intensity of light compared with optical tweezers. In addition, OET is particularly well suited for massively parallel manipulation schemes.^[4,24,30]

Although OT and OET are well-developed technologies with excellent precision and versatility for micromanipulation, they have potential shortcomings that limit their use for some applications. First, both techniques can cause physiological damage to trapped cells, by optical-induced heating from OT and photocurrent-induced Joule heating from OET.^[36–38] Second, in a standard micromanipulation platform that contains many micro-objects (beads, cells, etc.), it is challenging to generate a “clear” region that contains only the trapped micro-objects. Thus, when applying either technique to manipulate targeted particles in crowded environments, there is often unwanted physical/chemical/biological interference from other micro-objects in the field of view. Third, in both techniques, to maintain continuous application of the trapping force, the light source must always be “on.” This exacerbates the heating problem, and can also increase the evaporation rate of the liquid medium, thus altering the concentration of solutes and causing undesirable evaporation-induced fluidic shear forces. These challenges are substantial and are at least part of the reason that optical micromanipulation techniques are (currently) relegated to niche applications in research labs.

Here, we report a potential solution to the problems described above that we call “patterned OET” (p-OET). In p-OET, the photoconductive layer on a conventional OET device is patterned to allow convenient integration of OET with conventional DEP. The new p-OET format permits flexible, light-pattern-driven manipulation of particles/cells across an *X–Y* plane (as is the case for conventional OET), but also includes micropatterns in the photoconductive coating that permit continuous trapping of particles and cells by DEP, even after the light source is turned “off.” To our knowledge, this system is the first of its kind and has not been previously reported. In the conditions described here, the forces exerted by the patterned photoconductor were found to be useful a) to push away unwanted particles/cells (allowing for a clear field of experimentation), and b) to keep the particles/cells immobilized for long periods of time. In essence, p-OET allows the user to couple the unique features of OET with additional functionalities that do not require constant illumination, all on an integrated platform. We propose that p-OET may find use in a wide range of applications in the rapidly growing area of micromanipulation.

2. Results and Discussion

2.1. Optoelectronic Tweezers and Patterned Optoelectronic Tweezers

Figure 1 depicts the instrument and representative devices used in OET and p-OET. As shown in **Figure 1a**, a digital micro-mirror device (DMD) projector generates light patterns that are projected through the objective of an upright microscope onto a p-OET device. A long-pass filter removes blue wavelengths from the image prior to projecting into the microscope, and a short-pass filter in front of the camera reduces the intensity of the red emission from the projector, allowing a clear view of manipulated particles/cells juxtaposed with a faint pattern of the projected light. A function generator and amplifier provide AC potential to drive the OET and p-OET forces. Device position is controlled by a motorized positioning stage. The motorized positioning stage, DMD projector and CCD camera are controlled by the same computer, allowing centralized control and monitoring of the system.

As shown in **Figure 1b**, OET devices are made up of a top and bottom plate, each formed from a glass slide coated on one side with a thin layer of indium tin oxide (ITO). The bottom-plate ITO electrode is covered with a layer of 1 μm thick hydrogenated amorphous silicon (a-Si:H). In p-OET devices, the a-Si:H layer was etched to form patterns, as illustrated in **Figure 1c–g**. After fabrication, devices were assembled by joining a top and bottom plate (**Section S1** and **Figure S1**, Supporting Information) with a spacer to form a chamber, within which the manipulation of particles/cells was performed.

Conventional OET devices are functional because of the unique characteristics of the photoconductive a-Si:H coating. In the dark, the impedance of the a-Si:H layer is very high and the applied AC potential drops across this layer (leaving the liquid above mostly field-free). However, when the device is illuminated by light, the impedance of the photoconductive layer is reduced significantly, such that the voltage drops predominantly across the liquid medium above the illuminated area. The resulting nonuniform electric field in the medium interacts with the samples in the liquid medium producing either repulsive (negative DEP) or attractive (positive DEP) force depending on the Clausius–Mossotti (CM) factors of the system.^[39] Micro-objects with similar CM factors (i.e., those with similar material properties and operating conditions) behave similarly in OET systems, and the technique has been applied to manipulate micro-objects with a wide range of different materials, sizes, and shapes.^[4,20,26–28,40,41] **Figure 2a,b** illustrates the process of patterning 10 μm diameter polystyrene beads in a standard OET device (without micropatterns) to form an “Einstein” cartoon pattern at an AC potential of 7 $V_{\text{p-p}}$ at 25 kHz. The polystyrene beads experience negative DEP force and move away from the illuminated regions. As shown in **Figure 2c**, the pattern persists for a short time after the light is turned off, but as time passes (**Figure 2d–f**), the pattern gradually degrades and becomes unrecognizable.

The sequence of images in **Figure 2d–f** illustrates a common problem in optical micromanipulation. It is desirable to limit the duration of illumination to avoid potentially deleterious effects to

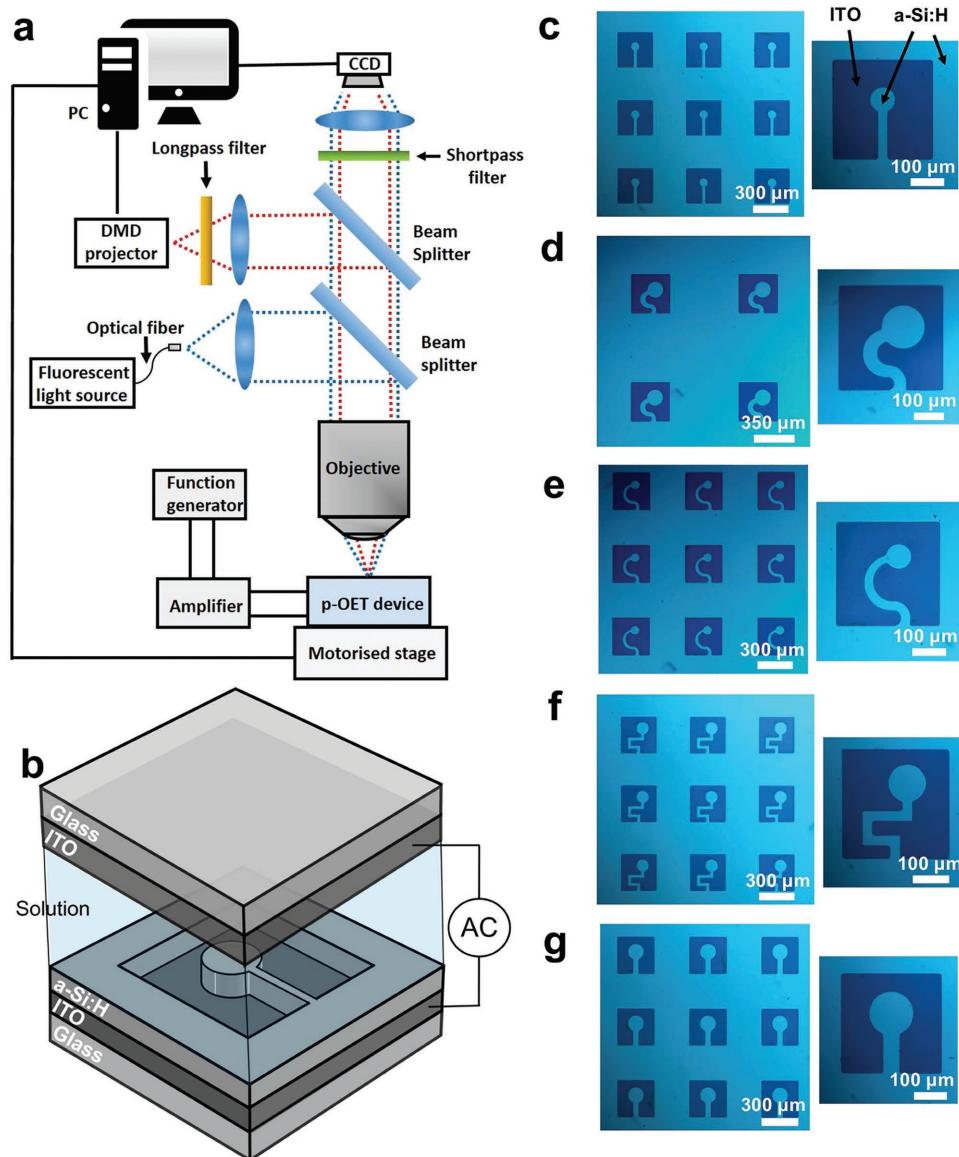


Figure 1. Experimental setup and device structure. a) Schematic of the experimental setup. b) 3D schematic of a portion of a p-OET device with a patterned hydrogenated amorphous silicon (a-Si:H) layer on an indium tin oxide (ITO) electrode. c–g) Bright-field microscope images of p-OET devices bearing arrays of patterned a-Si:H (which appear light) on ITO (which appear dark) (left) and magnified images of individual units in each array (right).

the trapped micro-objects. For example, as indicated in Section S2 and Figure S2 (Supporting Information), long-term illumination in this type of system can lead to a significant increase in the temperature and observed evaporation rate, conditions that are known to have a negative effect on cell health.^[36–38] However, when the light is turned “off,” objects in the device are subject to competing forces (Brownian motion, diffusion, fluid movement effects, etc.) that “undo” the work of the manipulation. This phenomenon led us to develop the new device format of p-OET.

2.2. Particle Behavior in p-OET Manipulations

In preparation for characterizing particle behavior in a p-OET device (with patterned photoconductor layer), we first

developed and characterized a conventional OET system (without patterning the photoconductor layer)—a “doughnut”-shaped OET trap.^[34,42] The trap used here has an inner radius of 80 μm and an outer radius of 150 μm , such that a single polystyrene particle can be trapped in the central (nonilluminated) region, confined within the circular ring of light by negative DEP. To calibrate the force applied to a particle in this trap, a series of experiments were completed in which the stage velocity was gradually increased to control the speed of the trapped particle. For example, **Figure 3a,b** shows representative microscope images of a 25 μm diameter polystyrene bead in the OET doughnut-trap travelling at 60 and 10 $\mu\text{m s}^{-1}$, respectively. As shown, the bead moves toward the edge of the light pattern as the velocity increases, confirming that a stronger DEP force is exerted to balance the increasing viscous

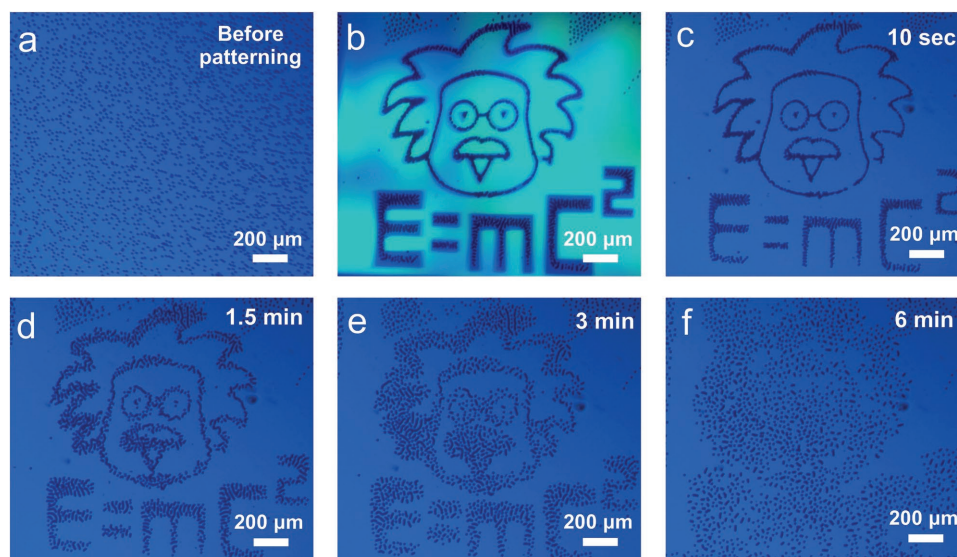


Figure 2. OET formation of a light-induced pattern in a suspension of polystyrene beads. a) Bright-field microscope image of an unpatterned suspension of 10 μm diameter beads (prior to illumination). b) Bright-field microscope image collected during illumination with a light pattern depicting a negative of a stylized cartoon of Albert Einstein and the mass-energy equation. c) Bright-field microscope image of the beads after patterning, 10 s after illumination. d–f) Bright-field microscope images of the beads 1.5, 3, and 6 min after patterning, illustrating the degradation of the pattern with time. The device was driven at $7 V_{p-p}$ (25 kHz).

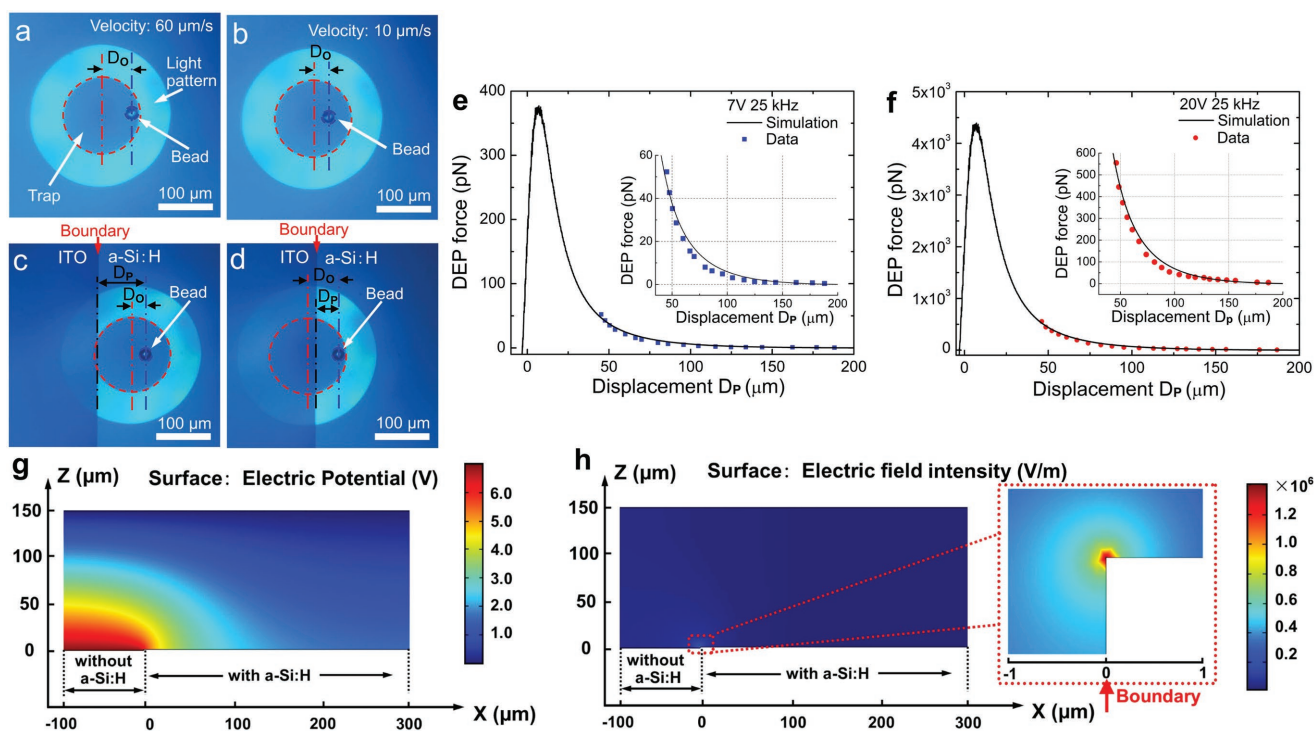


Figure 3. Patterned optoelectronic tweezers, p-OET. Bright-field microscope images of a 25 μm diameter bead moved by a doughnut-shaped OET trap at a) 60 $\mu\text{m s}^{-1}$ and b) 10 $\mu\text{m s}^{-1}$. D_0 denotes the distance between the bead center and the center of the OET trap. c,d) Bright-field microscope images of a 25 μm diameter bead in an OET trap moving at 2 $\mu\text{m s}^{-1}$ toward a linear boundary of exposed ITO (red arrows). D_p denotes the distance between the bead center and the edge of the p-OET feature. e–f) Measured DEP force profiles (blue squares and red circles) and simulated DEP force profiles (solid black lines) for a 25 μm diameter polystyrene bead in an OET trap while it is being repelled by a p-OET boundary when the device is driven e) at $7 V_{p-p}$ and f) at $20 V_{p-p}$ (25 kHz). The insets are magnified views of the region of the curve in which measurements were collected; at smaller D_p than is shown in the insets, the beads were observed to escape the OET trap. Simulated distribution of g) electric potential and h) electric field of p-OET device when it is driven at an AC potential of $7 V_{p-p}$, with heat maps from low (blue) to high (red) potential and field, respectively. The inset in panel (h) is a magnified portion of the boundary between exposed ITO (left) and ITO coated with a-Si:H (right).

drag force, allowing the bead to maintain a larger velocity (see Movie S1 in the Supporting Information). Stated another way, when velocity is increased, the bead moves closer to the edge of the light pattern, a phenomenon that can be quantified by the center-to-center displacement in the OET trap, “ D_O .” We characterized the force-profiles of the OET trap with experiments and simulations; beads manipulated by the trap in this work behave similarly to beads manipulated by OET traps described previously.^[30,34,42] The details of the model and the parameters that were used are described in Section S3 (and featured in Figure S3) in the Supporting Information.

Armed with a well-characterized OET doughnut-trap (Figure 3a,b), we turned to p-OET, in which we introduce a new condition by forming permanent, physically patterned windows through the photoconductor to expose the electrode below. These regions of the device are in essence always “on,” regardless of the state of the projected light. To study the properties of p-OET, a new series of experiments was completed in which a 25 μm diameter polystyrene bead was trapped by the OET doughnut-trap and was moved from a region coated with a-Si:H perpendicularly toward a linear boundary of exposed ITO (i.e., a simple p-OET feature). The OET doughnut-trap movement velocity in these experiments was low (2 $\mu\text{m s}^{-1}$); thus, under standard OET conditions, the bead remains near center of the OET trap (with small D_O). This behavior changes when the bead is driven toward the p-OET feature. We assigned a new parameter, “ D_p ” to quantify the distance between the center of the bead and the edge of the exposed ITO to evaluate this change in behavior. Figure 3c,d shows microscope images of the bead as the OET doughnut-trap is moved toward the exposed ITO, with $D_p = 100 \mu\text{m}$ (when the bead is far from the boundary) and $D_p = 46 \mu\text{m}$ (when the bead is closer to the boundary), respectively. As shown, as the bead gets closer to the exposed ITO, it experiences a stronger DEP force from boundary of the exposed ITO and is pushed away from the center of the OET doughnut-trap (Movie S2, Supporting Information). That is, as D_p is made to decrease (by moving the microscope stage to control the OET doughnut-trap), D_O increases, under conditions in which (with no exposed ITO) D_O would otherwise remain small and constant. The change in D_O in these experiments must be a result of the competition between the OET force in the light pattern and the DEP force generated at the boundary of the exposed ITO.

As indicated above, the force generated by an OET light pattern on a bead can be calculated based on the trap profile and the position of the bead in the trap (Figure S3, Supporting Information), which can, in turn, allow the calculation of the DEP force generated by the exposed ITO boundary. Therefore, a force profile can be plotted for the bead when it has different displacement D_p resulting from being close to the p-OET feature. Figure 3e,f shows the force profiles measured for a 25 μm diameter bead at different displacements with respect to the ITO/a-Si:H boundary when the p-OET device is driven at 7 V_{p-p} (blue squares) and 20 V_{p-p} (red circles), respectively. As shown, the DEP force generated by the ITO/a-Si:H boundary increases as the displacement D_p decreases, indicating that the DEP force repelling the bead increases as it approaches the ITO/a-Si:H boundary. To our knowledge, the data in Figure 3 represent the first report of a combination of conventional OET (the doughnut-shaped trap) and p-OET (the edge of the exposed ITO).

To better understand the observed experimental results, numerical simulations were carried out in COMSOL Multiphysics based on a well-developed 2D simulation model^[30,32,41,43] (with details and parameters included in Section S4 in the Supporting Information). The model includes the XZ cross-section of the p-OET device, and Figure 3g shows the simulated electrical potential distribution in the p-OET device. As shown in the simulation, there is a large electric potential variation along the Z-axis above the region without the a-Si:H layer, caused by the conductivity difference between ITO and a-Si:H. This effect also induces a large electric potential variation along the X-axis at the ITO/a-Si:H boundary region above the bottom surface. Figure 3h shows the simulated electrical field distribution in the p-OET device. As shown in the simulation, there exist strong electric fields (above $1 \times 10^6 \text{ V m}^{-1}$) and field variations at the ITO/a-Si:H boundary. The force profiles of the bead at different displacements with respect to the ITO/a-Si:H boundary were simulated using classic DEP theory and the dipole approximation method,^[30,31,39,43] as shown in Figure 3c,d (solid line). After scaling (Section S4, Supporting information), the simulation has a good qualitative match to the data, suggesting that there exists a strong DEP force to repel the bead at the ITO/a-Si:H boundary caused by a non-uniform electric field.

2.3. Applying OET and p-OET to Clear, Select, and “Trap” Beads

We next turned our attention to more complex p-OET “traps” in which devices were patterned to feature a-Si:H projections surrounded by exposed ITO (Figure 4a). A 3D model^[44] was developed to simulate this system, with length (X-axis) and width (Y-axis) set to 250 μm and height (Z-axis) set to 150 μm (Section S4, Supporting Information). Electric potential and electric field distributions were simulated and are shown in Figure 4b,c, respectively (XY-slices at $Z = 1.3 \mu\text{m}$, i.e., for a bead located 0.1 μm above the a-Si:H layer). As indicated, the electric potential varies significantly at the region near the ITO/a-Si:H boundary, inducing a strong electric field gradient directly over the boundary. This 3D model is consistent with the 2D simulations shown in Figure 3g,h, indicating there exists a strong DEP force surrounding the p-OET trap, both “inside” (along the inner edges of the exposed ITO, adjacent to the a-Si:H projection) and “outside” (around the outer edges of the exposed ITO) of the pattern. Stated another way, negative DEP forces exist that repel beads from the inner boundaries of the patterned ITO features and also from the outer boundaries of the ITO features. As shown in Figure 4d, when a p-OET trap was exposed to 20 μm diameter polystyrene beads outside of the trap, the beads were repelled from the outer ITO/a-Si:H boundary because of the negative DEP force. This illustrates a useful function for p-OET—the capacity to clear regions of the device of unwanted particles (e.g., beads or cells), keeping the patterns free for “trapping.” This concept of “clearing” the field of view is made much clearer in Movie S3 in the Supporting Information, in which beads are removed from the field by translating the microscope stage and device (which bears p-OET features) relative to stationary OET features.

Given its feasibility, we next combined the OET (mobile) “doughnut” trap with a p-OET (permanent) trap to select and

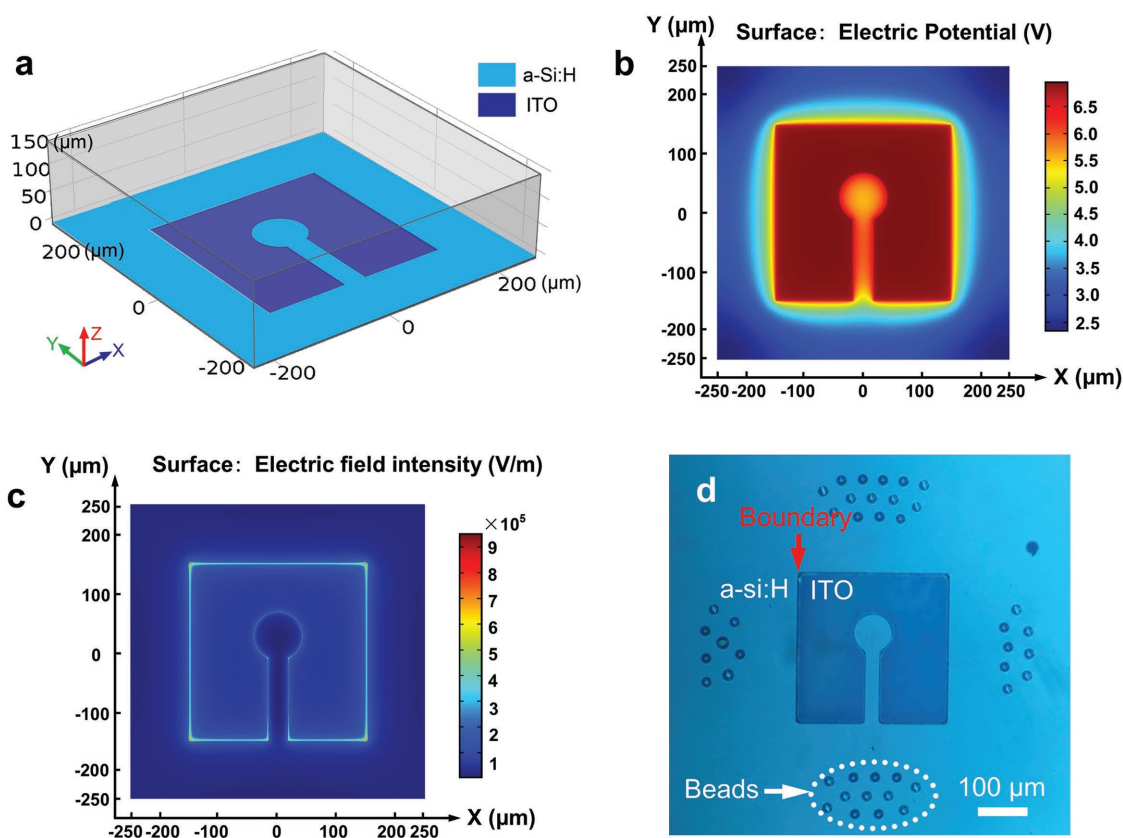


Figure 4. p-OET traps. a) 3D model of a p-OET trap in which a projection of a-Si:H is surrounded by exposed ITO. XY-plots at $Z = 1.3 \mu\text{m}$ of b) simulated electric potential distribution and c) electric field distribution for a device driven at $7 V_{p-p}$ (25 kHz), in which the simulated electric potential and field are indicated in heat maps (blue = low, red = high). d) Bright-field microscope image of device and conditions identical to the model in panels (a–c) showing the influence of the outer boundary of p-OET trap on $20 \mu\text{m}$ diameter beads located outside of the trap.

move individual beads into the center of the micropattern using the light-induced DEP force. **Figure 5a** shows a microscope image of a $15 \mu\text{m}$ diameter bead in an OET doughnut-trap outside of a p-OET trap. **Figure 5b** shows a microscope image of the same bead after it has been moved into the center of the p-OET trap, with a dashed line indicating the path that was taken. To accomplish this task, the microscope stage was programmed to follow the indicated path. As shown in Movie S4 in the Supporting Information, the movement of the OET doughnut-trap does not have to perfectly track the path of the p-OET trap—after being moved onto the a-Si:H projection, the bead “snaps” into the center of the path and remains there, presumably avoiding high negative DEP forces along the edges. As indicated in **Figure 5c,d**, by repeating this process, multiple beads can be moved into the same p-OET trap along the same track. After the beads are moved into the p-OET trap, they are preserved and confined even after the projector was turned off. This confinement is enabled by the “always on” DEP force generated by the circular ITO/a-Si:H boundary of the trap.

Figure 5e–l is a compendium of representative microscope images demonstrating the capacity to select and store multiple beads in p-OET traps with different geometries (using the same techniques indicated in **Figure 5a,b**). As shown, the beads adopt symmetrical patterns centered in the middle of the circular portion of the trap. This effect is reproducible—when the same

number of beads is stored in a trap with the same geometry, the resulting shape adopted by the beads is the same. We speculate that the shapes formed are determined by the distribution of the DEP force on the central (circular) pad. This region of the device can be modeled as a potential well with the energy level gradually decreasing from the edge (i.e., the interface between exposed ITO and the a-Si:H pattern) to the center. A single bead in the trap can be approximately regarded as an electric dipole, which positions itself at the minimum energy level near the center of the central pad. When multiple beads are moved onto the same trap, they form a multidipole system with each dipole being influenced not only by the edge of the central pad but also by the other dipoles in the system. Thus, the multidipole system reproducibly arranges itself to reach an electrostatic equilibrium, keeping the energy of the system at the minimum level. Future study of this effect is warranted (including the potential influence of electrohydrodynamic flow), but we propose that the self-assembly of beads into symmetrical patterns may someday be useful for making photonic crystals or plasmonic structures.^[45–48]

Finally, p-OET enables selection and sorting of particles in a heterogeneous mixture. For example, **Figure 5m,n** shows microscope images collected before and after sorting a mixture of $6 \mu\text{m}$ diameter red fluorescent polystyrene beads and $20 \mu\text{m}$ diameter green fluorescent polystyrene beads. As shown by the bright-field and fluorescent images in **Figure 5o,p**, particles of the same

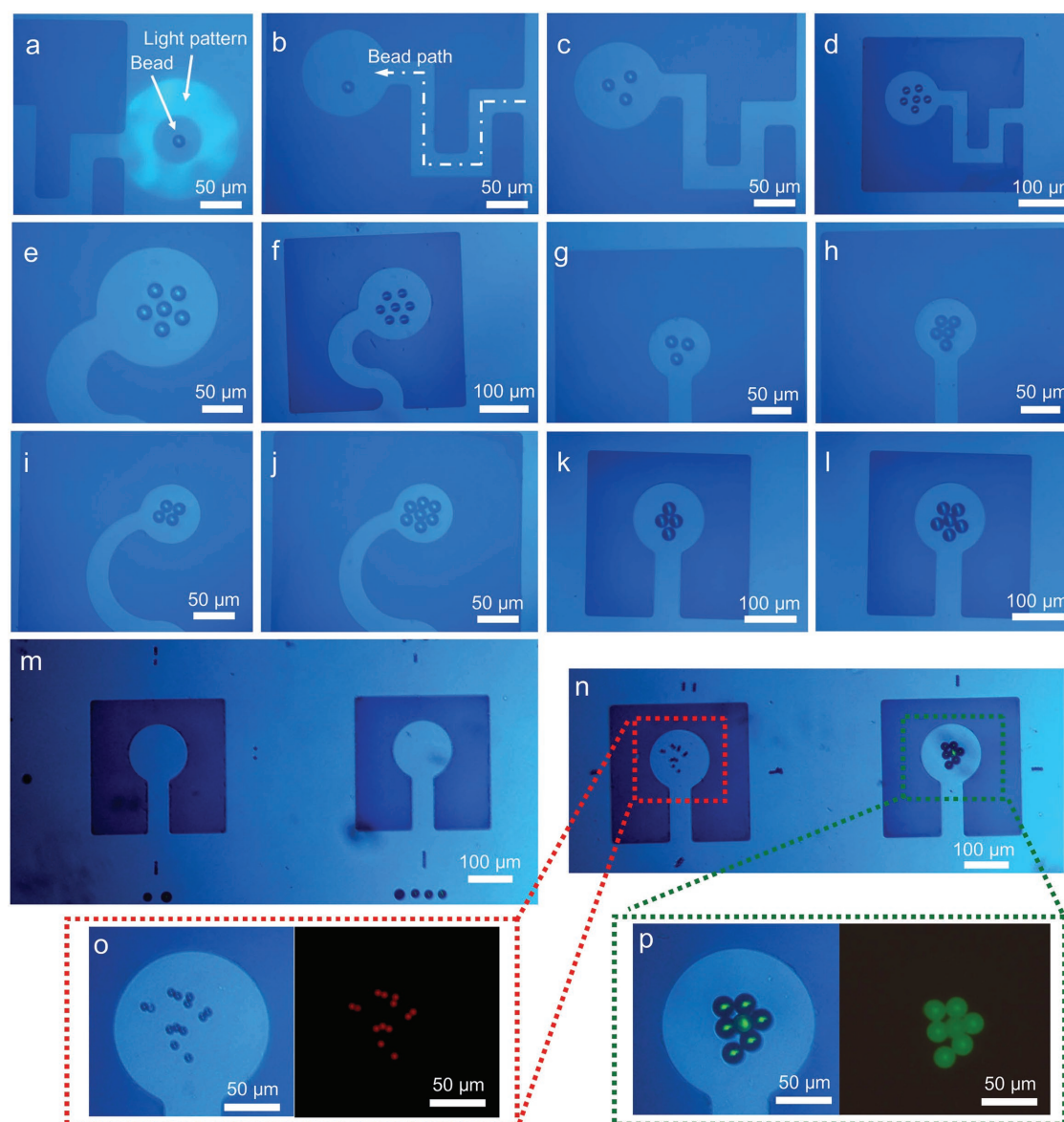


Figure 5. Selection and storage of beads in p-OET traps. a) Bright-field microscope image showing a 15 μm diameter polystyrene bead trapped by an OET doughnut-trap adjacent to the outer edge of a p-OET trap. b) Bright-field microscope image illustrating how the bead from panel (a) was transported into the trap. c,d) Microscope images showing the same trap from panel (b) after selecting and storing three and five beads, respectively. e–l) Bright-field microscope images of 15 μm diameter polystyrene beads selected and stored in various p-OET trap formats. Bright-field microscope images collected m) before and n) after selecting and sorting a mixture of two different types of particles (6 μm dia. red fluorescent polystyrene beads and 20 μm dia. green fluorescent polystyrene beads) into different p-OET traps. Magnified bright-field (left) and fluorescent microscope images (right) of o) 6 μm dia. beads and p) 20 μm dia. beads corresponding to panel (n). Additional formats and processes can be found in Movie S4 in the Supporting Information. All devices were driven at 20 V_{p-p} at 25 kHz.

kind can be selected and concentrated into designated p-OET traps. This capability suggests potential utility in the future for particle segregation and confinement,^[49] but in a manner that gives the user control to select the particles of interest.

2.4. Micromanipulation of Cells

OET has been heralded for its capability to precisely control the positions of mammalian cells.^[20] In this work, MCF-7 human

breast cancer cells and ARPE-19 human retinal pigment epithelial cells were used as a model system to evaluate this capability (for OET and p-OET). Under the conditions used here, these cells experience a negative light-induced DEP force (similar to the beads described above), such that they can be manipulated by the doughnut-shaped OET trap. Section S5, Figure S4, and Movie S5 in the Supporting Information illustrate some of the operations for manipulating cells that can be enabled using this OET system. As described herein, the “always on” nature of conventional OET is not ideal—it would

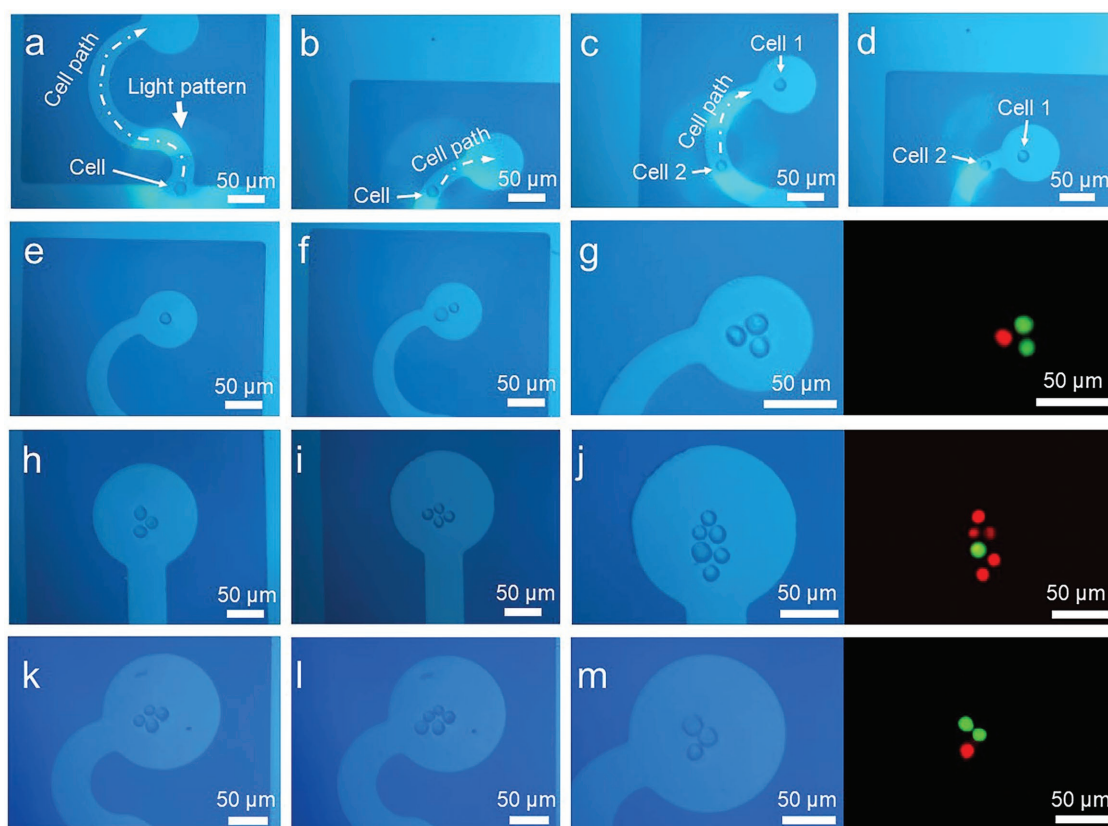


Figure 6. Selection and storage of MCF-7 breast cancer cells (prelabeled green by CellTracker dye) and ARPE-19 human retinal pigment epithelial cells (prelabeled red by CellTracker dye) in p-OET traps. a–d) Bright-field microscope images illustrating the movement of two cells (in series) onto the central pad of a p-OET trap. (e–m) Bright-field (left) and fluorescent microscope images (right) of varying cell patterns formed by moving cells (one-by-one) into the central pads of p-OET traps. Devices in these experiments were driven at 7 V_{p-p} (25 kHz). Additional examples of cell selection and storage in p-OET traps can be found in Movie S6 in the Supporting Information.

be useful to develop means to control cell position with or without illumination.

Figure 6a–d shows microscope images depicting the selection and movement (in OET doughnut-traps) of two cells that are then transferred and stored in a p-OET trap (Movie S6, Supporting Information). As is the case for dielectric beads, this method is useful for selection and storage of cells in p-OET traps with a variety of formats, as shown in the bright-field/fluorescent microscope images in Figure 6e–m. In some cases, a “half” doughnut light pattern was used for cell manipulation (Movie S6, Supporting Information), which minimized the effect of the illumination on cells that had previously been moved into the p-OET trap.

As shown, p-OET is a useful tool for selecting and isolating groups of mammalian cells. In the future, we propose that it may be appropriate for controlled cell mixing experiments to study biological processes such as entosis-mediated cell competition,^[50–54] whereby cancer cells invade proximate healthy cells, resulting in the death of the latter. Likewise, we propose that the tool may be useful to study processes such as immune cell interactions within cancer microenvironments,^[55,56] as well as immune cell–cancer cell interactions.^[57] Future users who attempt these and other applications involving cells will need to reconcile the difference between the low-conductivity

media (required for the techniques described here) and conventional, high-conductivity media that are typically used for long-term cell culture and maturation. Techniques for automated switching between high/low-conductivity media have been reported for OET^[21] and other techniques^[58] and we are confident that similar approaches could be developed for p-OET in the future.

Finally, as described herein, p-OET occupies a unique niche in that it (like OT and OET) allows for the generation of moveable, noncontact microparticle traps that give the user complete control over particle selection. Moreover, relative to OT and OET, p-OET has some advantages (long-term “always on” trapping without optical heating, capacity to clear a crowded field of view) and disadvantages (fabrication is more complex and some degree of flexibility is lost). But there are numerous other techniques that have been developed for similar applications, including magnetic tweezers (MT),^[59,60] DEP tweezers (DEPT),^[39,61–63] acoustic tweezers (AT),^[64,65] physical tweezers (PT),^[66,67] plasmonic optical tweezers (POT),^[68,69] and photovoltaic tweezers (PVT).^[70–72] Each of these methods has a unique combination of properties—for example, some techniques are purely “optical” but are limited to <nN trapping forces (OT, POT), other techniques enable application of >nN forces but require special measures to work with high-conductivity

media (OET, p-OET, PVT), others are innately compatible with high-conductivity media but require moving parts and physical contact with the trapped particles (MT, PT), and still others are useful for noncontact trapping of populations but are less well-suited for active selection of individual particles of interest (AT, DEPT). The savvy user will choose which technique is best suited to his or her application, or even better—he or she will adopt the emerging trend of combining different micromanipulation technologies together,^[20] to meet ever-more-demanding scientific challenges. We propose that the unique features of p-OET make it a welcome new addition to the micromanipulation toolbox, which may prove useful on its own or in tandem with other techniques for a wide range of applications.

3. Conclusions

In this work, we introduced a new method for manipulating dielectric particles and cells that we call patterned optoelectronic tweezers. p-OET is similar to conventional OET, except that the photoconductive layer that is typically continuous in an OET device is patterned, forming regions in which the electrode layer (below the photoconductor) is exposed. Systematic numerical simulations of these structures were carried out, which indicate that strong non-uniform electric fields exist at the edges of the exposed electrode layer. The simulation results were validated by experimental observations as the outer edges of patterns on the device were found to be useful for “pushing” beads and cells away from the area of interest. This solves a “particle-crowding” problem that exists for conventional OET and other techniques. Furthermore, we found that it is feasible to intentionally select and move beads or cells into a “trap” formed by a projection of photoconductor surrounded by exposed electrode material. Particles can be held in these traps by negative DEP without illumination, which solves another problem (light-induced heating) for OET and related techniques. As far as we are aware, the structures and effects presented here have not been reported previously, and we propose that this new tool may find use in a wide range of applications in the future.

4. Experimental Section

Device Fabrication and Operation: OET and p-OET devices comprise two plates (device shown in Figure S1a in the Supporting Information). The top plate is a glass slide coated on one side with 200 nm thick ITO (Riley Supplies). The bottom plate is formed from an ITO-coated glass slide, with the ITO layer coated with 1 μm thick a-Si:H, deposited by plasma enhanced chemical vapor deposition (Oxford Instruments Plasmalab 180 ICP-CVD system) from silane gas (30 sccm) at 250 °C with 10 W input power at 10 mTorr pressure. In p-OET devices, micropatterns in the a-Si:H layer were formed by standard photolithography and etching processes. Briefly, positive photoresist (Microposit S1818) was spin-coated onto the a-Si:H layer, and then exposed to UV light through a photomask to define the micropatterns. Substrates were then immersed in developer (Microposit MF-312) to form patterns in the photoresist. After rinsing, drying, and postbaking, the substrates were transferred to a ICP-RIE system (Oxford Instruments PlasmaPro-100 Cobra ICP-RIE System) to remove the a-Si:H (exposing ITO) in exposed regions using SF₆ gas (200 sccm flow rate, 1500 W ICP power, 20 W forward power,

20 mTorr pressure, 0 °C temperature; etch rate: 0.1 $\mu\text{m}/1.2$ s). After etching, the remaining photoresist was removed. Prior to assembly, the ≈ 2 mm² of the a-Si:H at the edge was removed with a blade to expose the conductive ITO layer. Electrical leads were interfaced with electrodes on the two plates via conductive silver paste (ALDRICH 735 825) and waterproof epoxy (Permatex 84 111). Devices were assembled by joining a top plate with a bottom plate by adhering them to a 150 μm thick spacer (3M 9965) to form an enclosed chamber (Figure S1b, Supporting Information). Finally, each device was affixed to a standard microscope glass slide (Figure S1c, Supporting Information) and was positioned in the slide holder of the microscope. In typical experiments, microobjects were manipulated by OET and p-OET by applying AC potentials ($7 V_{\text{p-p}}$, $20 V_{\text{p-p}}$, or $25 V_{\text{p-p}}$ at 25 kHz) between the top and bottom electrodes, respectively, with light patterns projected through a 10x objective. In most experiments, the light patterns were held stationary while the microscope stage (and device) was translated; in other experiments (Figure S4 and Movie S5, Supporting Information), the stage (and device) was held stationary while the light patterns were moved by the optical animations generated by PowerPoint. Both mechanisms (i.e., stationary-stage or stationary-light pattern) are useful and are commonly used in OET experiments.

Instrumentation: The OET system is shown in Figure 1a, which includes a digital micromirror device projector (Dell 1650), an upright fluorescent microscope (Leica DM 2000), a fluorescent excitation source (X-cite 120), a motorized stage (Märzhäuser Scan Plus 100 \times 100), a high-resolution stepper motor controller (Märzhäuser TANGO), a control joystick (Märzhäuser 3-axes joystick), an amplifier (Thurlby Thandor Instrument WA31), a function generator (Agilent 33220A), a charge-coupled device camera (LW Scientific MiniVID; TouptView image software) and a Desktop computer (Dell Optiplex 790). The filters in the system include a long-pass filter (Thorlabs FD1R) and a short-pass filter (Thorlabs FES0550). An infrared camera (FLIR E60) was used to measure the temperature profiles of the OET device. A power meter with a silicon photodiode detector (Thorlabs PM16-130) was used to measure the optical power from the projector. A conductivity meter (HACH H270G) and probe (HACH PH77-SS) was used to measure the conductivity of medium.

Preparation of Particle Suspension: Spherical polystyrene beads with diameters of 6, 10, 15, 20, and 25 μm (Polysciences) were suspended in deionized (DI) water containing 0.05% v/v Tween 20 (P9416 SIGMA). The conductivity of the suspension was measured to be 5.0 mS m⁻¹. In a typical experiment, a 15 μL of the suspension was pipetted into the chamber of the p-OET device.

Cell Culture and Fluorescent Labeling: MCF-7 cells were maintained in Dulbecco's modified Eagle's medium (DMEM; Life Technologies) supplemented with 10% v/v fetal bovine serum (FBS; Gibco) and 1% v/v penicillin and streptomycin (pen./strep., Invitrogen). ARPE-19 cells were maintained in DMEM/F12 media (Life Technologies) supplemented with 10% v/v FBS and 1% v/v pen./strep. Cells were incubated in a humidified 5% CO₂ air environment at 37 °C. Adherent cells were stained by adding 10×10^{-6} M CellTracker Green CMFDA or Red CMPTX (ThermoFisher Scientific), diluted in the cell line's base media in the absence of serum, and incubated for 30 min at 37 °C. Stained cells were then washed twice by addition of phosphate-buffered saline (PBS; Life Technologies), passaged using 0.25% Trypsin-EDTA (Life Technologies) and resuspended in sucrose media (9 wt% sucrose, 0.3 wt% D-Glucose, 1.25% v/v PBS; conductivity measured to be 22.1 mS m⁻¹) at a density of $0.1\text{--}1 \times 10^6$ cells mL⁻¹. After filtering the sucrose media containing cells through a 40 μm diameter pore strainer (Falcon), an aliquot of cell-suspension (15 μL) was pipetted into the chamber of the OET device for experiments.

Supporting Information

Supporting Information is available from the Wiley Online Library or from the author.

Acknowledgements

This research was supported by the Natural Sciences and Engineering Research Council of Canada (Grants RGPIN 2014-06042, CREATE 482073-16) and the National Natural Science Foundation of China (Grants 11774437, U1701661, 61490715). The research was also supported by the University of Toronto's Medicine by Design initiative, which receives funding from the Canada First Research Excellence Fund (CFREF). Finally, the authors acknowledge support from the Toronto Nanofabrication Centre at the University of Toronto for help with device fabrication; ARW and PWZ acknowledge the Canada Research Chair program for CRCs.

Conflict of Interest

The authors declare no conflict of interest.

Keywords

cell capture, dielectrophoresis, micropatterns, optical micromanipulation, optoelectronic tweezers

Received: August 17, 2018

Published online: October 11, 2018

- [1] A. Ashkin, J. M. Dziedzic, T. Yamane, *Nature* **1987**, 330, 769.
- [2] P. J. Pauzauskie, A. Radenovic, E. Trepagnier, H. Shroff, P. Yang, J. Liphardt, *Nat. Mater.* **2006**, 5, 97.
- [3] M. C. Zhong, X. B. Wei, J. H. Zhou, Z. Q. Wang, Y. M. Li, *Nat. Commun.* **2013**, 4, 1768.
- [4] P. Y. Chiou, A. T. Ohta, M. C. Wu, *Nature* **2005**, 436, 370.
- [5] M. C. Wu, *Nat. Photonics* **2011**, 5, 322.
- [6] A. Ashkin, J. M. Dziedzic, *Science* **1987**, 235, 1517.
- [7] S. M. Block, D. F. Blair, H. C. Berg, *Nature* **1989**, 338, 514.
- [8] G. Thalhammer, R. Steiger, S. Bernet, M. Ritsch-Marte, *J. Opt.* **2011**, 13, 044024.
- [9] W. Choi, S. W. Nam, H. Hwang, S. Park, J. K. Park, *Appl. Phys. Lett.* **2008**, 93, 143901.
- [10] G. Leitz, E. Fällman, S. Tuck, O. Axner, *Biophys. J.* **2002**, 82, 2224.
- [11] M. D. Wang, H. Yin, R. Landick, J. Gelles, S. M. Block, *Biophys. J.* **1997**, 72, 1335.
- [12] A. H. J. Yang, S. D. Moore, B. S. Schmidt, M. Klug, M. Lipson, D. Erickson, *Nature* **2009**, 457, 71.
- [13] M. Z. Hoeb, J. O. Rädler, S. Klein, M. Stutzmann, M. S. Brandt, *Biophys. J.* **2007**, 93, 1032.
- [14] Y. H. Lin, C. M. Chang, G. B. Lee, *Opt. Express* **2009**, 17, 15318.
- [15] X. Wang, S. Chen, M. Kong, Z. Wang, K. D. Costa, R. A. Li, D. Sun, *Lab Chip* **2011**, 11, 3656.
- [16] M. M. Wang, E. Tu, D. E. Raymond, J. M. Yang, H. Zhang, N. Hagen, B. Dees, E. M. Mercer, A. H. Forster, I. Kariv, P. J. Marchand, *Nat. Biotechnol.* **2005**, 23, 83.
- [17] H. Xin, Y. Li, B. Li, *Adv. Funct. Mater.* **2015**, 25, 2816.
- [18] A. T. Ohta, M. Garcia, J. K. Valley, L. Banie, H.-Y. Hsu, A. Jamshidi, S. L. Neale, T. Lue, M. C. Wu, *Lab Chip* **2010**, 10, 3213.
- [19] S. M. Yang, T. M. Yu, H. P. Huang, M. Y. Ku, L. Hsu, C. H. Liu, *Opt. Lett.* **2010**, 35, 1959.
- [20] H. Hwang, J. K. Park, *Lab Chip* **2011**, 11, 33.
- [21] L. Y. Ke, Z. K. Kuo, Y. S. Chen, T. Y. Yeh, M. Dong, H. W. Tseng, C. H. Liu, *Lab Chip* **2018**, 18, 106.
- [22] A. Ashkin, J. M. Dziedzic, J. E. Bjorkholm, S. Chu, *Opt. Lett.* **1986**, 11, 288.
- [23] D. G. Grier, *Nature* **2003**, 424, 810.
- [24] M. Woerdemann, C. Alpmann, M. Esseling, C. Denz, *Laser Photonics Rev.* **2013**, 7, 839.
- [25] M. Daly, M. Sergides, S. N. Chormaic, *Laser Photonics Rev.* **2015**, 9, 309.
- [26] A. Jamshidi, P. J. Pauzauskie, P. J. Schuck, A. T. Ohta, P. Y. Chiou, J. Chou, P. Yang, M. C. Wu, *Nat. Photonics* **2008**, 2, 86.
- [27] P. J. Pauzauskie, A. Jamshidi, J. K. Valley, J. H. S. Jr., M. C. Wu, *Appl. Phys. Lett.* **2009**, 95, 113104.
- [28] A. Jamshidi, S. L. Neale, K. Yu, P. J. Pauzauskie, P. J. Schuck, J. K. Valley, H. Y. Hsu, A. T. Ohta, M. C. Wu, *Nano Lett.* **2009**, 9, 2921.
- [29] S. L. Neale, A. T. Ohta, H. Y. Hsu, J. K. Valley, A. Jamshidi, M. C. Wu, *Opt. Express* **2009**, 17, 5231.
- [30] S. L. Neale, M. Mazilu, J. I. B. Wilson, K. Dholakia, T. F. Krauss, *Opt. Express* **2007**, 15, 12619.
- [31] S. B. Huang, M. H. Wu, Y. H. Lin, C. H. Hsieh, C. L. Yang, H. C. Lin, C. P. Tseng, G. B. Lee, *Lab Chip* **2013**, 13, 1371.
- [32] S. Zhang, J. Juvert, J. M. Cooper, S. L. Neale, *Sci. Rep.* **2016**, 6, 32840.
- [33] S. Ota, S. Wang, Y. Wang, X. Yin, X. Zhang, *Nano Lett.* **2013**, 13, 2766.
- [34] A. T. Ohta, P. Y. Chiou, T. H. Han, J. C. Liao, U. Bhardwaj, E. R. B. McCabe, F. Yu, R. Sun, M. C. Wu, *J. Microelectromech. Syst.* **2007**, 16, 491.
- [35] H. Y. Hsu, A. T. Ohta, P. Y. Chiou, A. Jamshidi, S. L. Neale, M. C. Wu, *Lab Chip* **2010**, 10, 165.
- [36] K. C. Neuman, E. H. Chadd, G. F. Liou, K. Bergman, S. M. Block, *Biophys. J.* **1999**, 77, 2856.
- [37] M. B. Rasmussen, L. B. Oddershede, H. Siegmundfeldt, *Appl. Environ. Microbiol.* **2008**, 74, 2441.
- [38] S. M. Yang, S. Y. Tseng, H. P. Chen, L. Hsu, C. H. Liu, *Lab Chip* **2013**, 13, 3893.
- [39] R. Pethig, *Biomechanics* **2010**, 4, 022811.
- [40] J. Juvert, S. Zhang, I. Eddie, C. J. Mitchell, G. T. Reed, J. S. Wilkinson, A. Kelly, S. L. Neale, *Opt. Express* **2016**, 24, 18163.
- [41] S. Zhang, Y. Liu, J. Juvert, P. Tian, J. C. Navarro, J. M. Cooper, S. L. Neale, *Appl. Phys. Lett.* **2016**, 109, 221110.
- [42] S. L. Neale, M. C. Wu, presented at *Conference on Lasers and Electro-Optics (p. CThLL6)*, San Jose, California, United States, May **2008**.
- [43] S. Xie, X. Wang, N. Jiao, S. Tung, L. Liu, *Lab Chip* **2017**, 17, 2046.
- [44] S. Zhang, A. Nikitina, Y. Chen, Y. Zhang, L. Liu, A. G. Flood, J. Juvert, M. D. Chamberlain, N. P. Kherani, S. L. Neale, A. R. Wheeler, *Opt. Express* **2018**, 26, 5300.
- [45] J. Li, S. Dong, J. Tong, P. Zhu, G. Diao, Z. Yang, *Chem. Commun.* **2016**, 52, 284.
- [46] K. Liu, Y. Tian, Q. Li, X. Y. Du, J. Zhang, C. F. Wang, S. Chen, *J. Mater. Chem. C* **2018**, 6, 2336.
- [47] J. Chen, Y. Sun, L. Zhong, W. Shao, J. Huang, F. Liang, Z. Cui, Z. Liang, L. Jiang, L. Chi, *Small* **2016**, 12, 5818.
- [48] I. Elvira, J. F. Muñoz-Martínez, Á. Barroso, C. Denz, J. B. Ramiro, A. García-Cabañes, F. Agulló-López, M. Carrascosa, *Opt. Lett.* **2018**, 43, 30.
- [49] D. D. Carlo, J. F. Edd, K. J. Humphry, H. A. Stone, M. Toner, *Phys. Rev. Lett.* **2009**, 102, 094503.
- [50] M. Overholtzer, A. A. Mailleux, G. Mouneimne, G. Normand, S. J. Schnitt, R. W. King, E. S. Cibas, J. S. Brugge, *Cell* **2007**, 131, 966.
- [51] E. White, *Cell* **2007**, 131, 840.
- [52] M. Overholtzer, J. S. Brugge, *Nat. Rev. Mol. Cell Biol.* **2008**, 9, 796.
- [53] A. Janssen, R. H. Medema, *Nat. Cell Biol.* **2011**, 13, 199.
- [54] G. Kroemer, J. L. Perfettini, *Cell Res.* **2014**, 24, 1280.
- [55] F. S. Varn, Y. Wang, D. W. Mullins, S. Fiering, C. Cheng, *Cancer Res.* **2017**, 77, 1271.
- [56] H. Dong, S. E. Strome, D. R. Salomao, H. Tamura, F. Hirano, D. B. Flies, P. C. Roche, J. Lu, G. Zhu, K. Tamada, V. A. Lennon, C. Esteban, L. Chen, *Nat. Med.* **2002**, 8, 793.

- [57] D. Pettitt, Z. Arshad, J. Smith, T. Stanic, G. Holländer, D. Brindley, *Mol. Ther.* **2018**, 26, 342.
- [58] S. C. C. Shih, I. Barbulovic-Nad, X. Yang, R. Fobel, A. R. Wheeler, *Biosens. Bioelectron.* **2013**, 42, 314.
- [59] M. M. Van Oene, L. E. Dickinson, B. Cross, F. Pedaci, J. Lipfert, N. H. Dekker, *Sci. Rep.* **2017**, 7, 43285.
- [60] I. D. Vlaminc, Cees Dekker, *Annu. Rev. Biophys.* **2012**, 41, 453.
- [61] H. Song, J. M. Rosano, Y. Wang, C. J. Garson, B. Prabhakarpandian, K. Pant, G. J. Klarmann, A. Perantoni, L. M. Alvarez, E. Lai, *Lab Chip* **2015**, 15, 1320.
- [62] S. Y. Tang, J. Zhu, V. Sivan, B. Gol, R. Soffe, W. Zhang, A. Mitchell, K. Khoshmanesh, *Adv. Funct. Mater.* **2015**, 25, 4445.
- [63] R. J. Barsotti, M. D. Vahey, R. Wartena, Y. M. Chiang, J. Voldman, F. Stellacci, *Small* **2007**, 3, 488.
- [64] X. Ding, S. C. S. Lin, B. Kiraly, H. Yue, S. Li, I. K. Chiang, J. Shi, S. J. Benkovic, T. J. Huang, *Proc. Natl. Acad. Sci. USA* **2012**, 109, 11105.
- [65] J. P. Lata, F. Guo, J. Guo, P. H. Huang, J. Yang, T. J. Huang, *Adv. Mater.* **2016**, 28, 8632.
- [66] Z. Gong, B. K. Chen, J. Liu, Y. Sun, *IEEE Trans. Rob.* **2014**, 30, 758.
- [67] Z. R. Zhang, J. Liu, X. Wang, Q. L. Zhao, C. Zhou, M. Tan, H. Y. Pu, S. R. Xie, Y. Sun, *IEEE Rob. Autom. Lett.* **2017**, 2, 570.
- [68] C. Min, Z. Shen, J. Shen, Y. Zhang, H. Fang, G. Yuan, L. Du, S. Zhu, T. Lei, X. Yuan, *Nat. Commun.* **2013**, 4, 2891.
- [69] K. Wang, E. Schonbrun, P. Steinvurzel, K. B. Crozier, *Nat. Commun.* **2011**, 2, 469.
- [70] J. F. Muñoz-Martínez, I. Elvira, M. Jubera, A. García-Cabañes, J. B. Ramiro, C. Arregui, M. Carrascosa, *Opt. Mater. Express* **2015**, 5, 1137.
- [71] M. Carrascosa, A. García-Cabañes, M. Jubera, J. B. Ramiro, F. Agulló-López, *Appl. Phys. Rev.* **2015**, 2, 040605.
- [72] A. García-Cabañes, A. Blázquez-Castro, L. Arizmendi, F. Agulló-López, M. Carrascosa, *Crystals* **2018**, 8, 65.